ACS OMEGA

http://pubs.acs.org/journal/acsodf

Article

Optimizing the Micro/Mesoporous Structure of Hierarchical Porous Carbon Synthesized from Petroleum Pitch Using the Solvent-Free Method for Ultra-Fast Capacitive Deionization

Guan-Wen Liu, Chen-Shiuan Fan, Chun-Han Hsu, Chia-Hung Hou,* and Hong-Ping Lin*

Cite This: *ACS Omega* 2022, 7, 47610−47618

Read Online

ACCESS | Metrics & More | Article Recommendations

ABSTRACT: In this work, a solvent-free ZnO-template method is used to synthesize hierarchical porous carbons (denoted as HPC-*X*; *X* = 1, 1.5, 2, and 4 g of ZnO) via the pyrolysis of petroleum industrial-residual pitch with ZnO. The proposed method allows precise control of the micro/meso/macroporous structure of the HPC by adjusting the amount of ZnO. The results show that the average pore size of HPCs prominently increases from 2.4 to 3.7 nm with the increase in the ZnO/pitch ratio. In addition, it is shown that HPCs have a high surface area between 1141 and 1469 $m^2 g^{-1}$, a wide-range pore size distribution (micro-, meso-, and macropores), and a tap density ranging from 0.2 to 0.57 g cm^{-3}. The capacitive deionization performances of HPCs for sodium and chloride ions are investigated. The results show that HPC-2 exhibits the highest electrosorption capacity of 9.94 mg g^{-1} within 10.0 min and a maximum electrosorption capacity of 10.62 mg g^{-1} at 1.2 V in a 5.0 mM NaCl solution. Hence, HPC-2 is a highly promising candidate as an electrode material for rapid deionization.

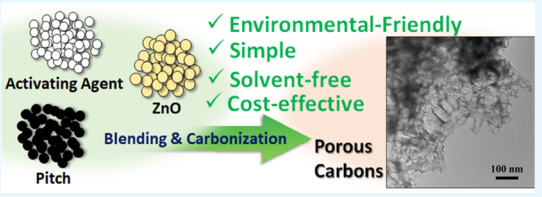

1. INTRODUCTION

Recently, capacitive deionization (CDI) is being developed as a potential method for water deionization because of its lower energy consumption, low pressure, and environment-friendly characteristics.[1−3] During the electrosorption process of CDI, which follows the electrical double layer (EDL) theory, ions are attracted to the oppositely charged electrodes by applying the electrical potential difference between two electrodes. When the voltage is removed, ions release from the electrodes back into the solution. In this case, CDI requires electrodes with high salt adsorption capacity (SAC) and salt adsorption rate (SAR) to store plentiful ions as quickly as possible during the deionization process.[4,5] In order to achieve those traits, the CDI electrodes should possess several characteristics: (i) large specific surface area for ion adsorption; (ii) high electrical conductivity; (iii) high electrochemical stability; and (iv) appropriate pore structure for rapid ion adsorption−desorption.[6−8]

Nowadays, carbon materials with the characteristics mentioned above are widely utilized as CDI electrodes.[7−12] Especially, hierarchical porous carbons (HPCs) with three-dimensional porous structures have become popular in the electrosorption field in recent years.[6,13−15] These materials allow for the adsorption of more charged species by their EDL under an applied potential and thus improve the SAC and SAR.[13−15] HPCs have been synthesized by various methods such as hard templating using silica with distinct structures or soft templating using a surfactant.[16−21] However, these traditional synthesis procedures are complicated, expensive, time-consuming, and toxic.[22,23] Hence, they cannot be commercialized. The development of simple, low-cost strategies for the synthesis of HPCs remains a significant challenge.

Accordingly, this study proposed a new synthesis method to achieve simplicity and cheapness. First, a solvent-free ZnO-template method which has been established in our previous work is used to synthesize HPCs with a high specific surface area and an optimized micro/mesoporous structure.[24] This synthesis method uses an inexpensive, commercially available ZnO template and a solvent-free process instead of a siliceous template and reaction in solution, respectively. It is, therefore, more simple, low-cost, and environmentally friendly.[24] Second, the petroleum industrial-residual pitch, which is presented ubiquitously on earth, is used as a cheaper alternative for the carbon precursor. It possesses abundant aromatic hydrocarbons, which can be polymerized and further aromatized to form carbons with a high carbon yield.[25−28] Moreover, traditionally, pitch is used as a low-efficiency fuel. When it is burned, it generates relatively little energy but emits a large amount of carbon dioxide, which severely aggravates climate change.[29−31] Therefore, in order to protect the environment,

Received: June 30, 2022
Accepted: November 22, 2022
Published: December 15, 2022

pitch is used as the carbon precursor in the method proposed in this study to produce high-value HPCs.

According to past research, the textural characteristics of carbon materials, such as the pore structure, pore size, and micro/mesopore volume, have significant connections with the electrosorption ability.[21,32−34] The presence of microporosity could effectively increase the specific surface area. Yet, the carbon materials with high microporosity usually exhibit low pore accessibility, which causes relatively low SAC since micropores would significantly inhibit ion penetration and limit mass transfer rates.[2,32] Furthermore, Lee et al. also showed that owing to the electrical EDL overlapping effect, the higher specific surface area almost donated from micropores does not contribute to the higher ion capacity.[35] Conversely, the mesoporosity could effectively utilize the surface area for ion storage, relieve ion transfer resistance, and enhance the ion electrosorption rate. Zhao et al. proved the superiority of mesoporous carbon with an ordered structure for its CDI ability.[20] However, mesoporous carbons also possess shortcomings, such as low specific surface area and low bulk density. Importantly, the high bulkiness which causes coating difficulty on the electrodes deeply limits their capability on CDI. Therefore, the appropriate micro/mesopores ratio of carbon materials is still needed to be investigated to enhance the SAC.

In most cases, the porosity of carbon materials is tailored through physical or chemical activation. However, those methods only create micropores and small mesopores.[36] They do not support the tailoring of pore sizes over a wide range. In addition, excessive activating agents also induce a significant decrease in carbon yield, which leads to economic drawbacks. Using siliceous templates with distinctive pore structures to synthesize carbon materials is another method to tailor their porosity. However, the procedures for the synthesis of different siliceous templates are so complex, time-consuming, high-cost, and environmentally unfriendly that they are not suitable to be utilized on a large scale.[22,23] Therefore, a new method needs to be established to address the current deficits caused by the application of activation processes and siliceous templates.

In this novel study, a new hierarchical porous carbon with high specific surface area and hierarchical pores was developed in our laboratory using petroleum industrial-residual pitch via a solvent-free ZnO-template method. Importantly, the porosity of HPCs is simply tailored to achieve an optimized micro/mesopores ratio by adjusting the ZnO/pitch ratio.[24] Through comparison of HPC-X (X = 1, 1.5, 2, and 4 g of ZnO) electrodes in electrochemical analysis, we reveal the effects of the pore size distribution (micropores and mesopores) on their performance for salt removal. Their excellent brackish water desalination capacities were quantified by batch-mode experiments. These results in this study could have a significant influence on the design of advanced porous carbons and CDI applications.

2. EXPERIMENTAL SECTION

2.1. Synthesis of Hierarchical Micro/Mesoporous Carbons. HPCs were synthesized using industry-residual petroleum pitch (CF19, softening point 120 °C, provided from Chinese Petroleum Corporation, Taiwan), ZnO (AZO900, Diamonchem International Co, Taiwan), and potassium hydroxide (KOH, purchased from Merck), as the carbon source, hard template, and activating agent, respectively. In performing the synthetic procedure, pitch, ZnO, and KOH were ground into a homogeneous mixture using a blender (SRT-02, S.SHIN CO., LTD, Taiwan) at 3000 rpm for 2 min with weight ratios of x/1.0/0.75, where x is the ZnO template weight (x = 1.0, 1.5, 2.0, and 4.0 g), 1.0 is the pitch weight (g), and 0.75 is the activating agent weight (g). The resulting powder was sealed in a stainless-steel vessel and then heated in a furnace. The heating rate was set at 8 °C min^{-1} and held at a carbonization temperature of 900 °C for 2 h. After cooling to room temperature, the products were treated with DI water first and then soaked in an appropriate amount of 3.0 M HCl solution under stirring for 2 h to remove the KOH and ZnO, respectively. The resulting samples (HPC) were dried in an air-oven at 100 °C for 12 h for further characterization.

2.2. Structural Characterization. Scanning electron microscopy (SEM) images of the porous carbons were recorded by a field emission scanning electron microscope (FE-SEM, JEOL JSM7000F, USA). Transmission electron microscopy (TEM) was conducted using a Hitachi H-7500 microscope. The tap density of the samples was obtained with a tap density analyzer. The N_2 adsorption−desorption isotherms of the samples were taken at 77 K on a micrometric Tristar II apparatus to estimate the pore size, pore volume, and surface area. The pore-size distribution curves were obtained from an analysis of the adsorption isotherms using the BJH (Barrett−Joyner−Halenda) method.

2.3. Electrochemical Measurement. A symmetrical two-electrode capacitor cell was used to examine the electrochemical performance of the porous carbon electrodes. Both electrodes were made by depositing ca. 1.0 mg carbons onto 1.0 cm^2 stainless foil, which acted as a current collector. The cell consisted of two carbon electrodes, sandwiching a cellulose filter paper as the separator.

Cyclic voltammetry (CV) measurements were conducted between 0 and 1.0 V in a 1.0 M NaCl solution at sweep rates ranging of 5 to 500 mV s^{-1}. Plots of the specific capacitance versus the voltage were calculated using the following formula

$$C = 2I/vm$$

where I is the current (A), v is the scan rate (V s^{-1}), and m denotes the mass (g) of the carbon material in one electrode.

To test the charge/discharge performance, the supercapacitor was charged with constant current (9 A g^{-1}) up to a voltage of 1.0 V, and then discharged with constant current (−9 A g^{-1}) down to a voltage of 0 V in 1.0 M NaCl solution. Electrochemical impedance spectroscopy (EIS) measurements were conducted at an open-circuit voltage (0 V) over the frequency range of 1 mHz−100 kHz with a 5 mV amplitude.

2.4. Preparation of Carbon Electrodes. HPC and polyvinylidene fluoride (PVDF, Porex, 99%) binder was used to fabricate carbon electrodes. HPC-1, HPC-1.5, and HPC-2 were used as electrode material to determine the optimum ZnO amount when synthesizing the HPC. N-methylpyrrolidone (NMP, Macron, 99.5%) was used as a solvent. Carbon electrodes were fabricated by mixing HPC (92.5 wt %), PVDF binder (7.5 wt %), and NMP for 2 h to ensure homogeneity. The carbon slurry was coated onto a titanium plate and then dried in an air-oven at 100 °C for 4 h to remove the organic solvent.

2.5. Electrosorption Experiments of Capacitive Deionization. Electrosorption experiments were performed in a batch-mode recycling system, in which the NaCl solution was continuously circulated through the CDI cell using a peristaltic pump at a flow rate of 10 mL min^{-1}. The CDI cell was

https://doi.org/10.1021/acsomega.2c04119
ACS Omega 2022, 7, 47610−47618

composed of two-sided carbon electrodes separated by a spacer with a distance of 2 mm to allow for solution flow. A voltage of 1.2 V was applied to the two oppositely charged electrodes by a CHI 6144C electrochemical analyzer. The concentration change of the solution was measured using an online conductivity meter (PL-700PCS). The electrosorption capacity (EC) was calculated by

$$EC = (C_0 - C_t)\, VM/m$$

where C_0 and C_t are the initial and equilibrated NaCl concentrations, respectively; V is the solution volume; M is the molecular weight of NaCl; m is the total mass of the electrode materials.

The electrosorption rate (ER) was calculated as

$$ER = EC/t$$

where EC is the electrosorption capacity, and t is the electrosorption time.

3. RESULTS AND DISCUSSION

3.1. Surface Morphology and Structural Characterization. Figure 1a,b presents the SEM images of the HPC-1 and HPC-4 samples, respectively. Figure 1a shows that many circular holes with diameters of 20−60 nm are formed on the surface of HPC-1, which demonstrates an almost perfect replication of the ZnO template shape. Compared with the pore structure of HPC-1, Figure 1b shows that HPC-4 involves more meso- and macropores. This finding is reasonable since the ZnO particles can leave spaces according to their volume after removal from the HPC via diluted $HCl_{(aq)}$. Therefore, as the ZnO/pitch ratio increases, the number of meso- and macropores in the pore structure of HPCs conspicuously increases. In other words, the pore size of the HPC can be effectively controlled by adjusting the ZnO/pitch ratio. Figure 1c,d shows the TEM images of the HPC-1 and HPC-4 samples, respectively. In Figure 1c, it seems that HPC-1 has an integrally hierarchical porous structure with a small number of mesopores as well as thick carbon walls. Conversely, Figure 1d shows that due to the higher ZnO/pitch ratio, more meso- and macropores are formed in the HPC-4 sample. Furthermore, Figure 1c,d show the obvious presence of micropores and smaller mesopores in the walls of large mesopores and macropores, which suggests that the smaller mesopores and micropores of the HPCs are well-connected via the meso- and macropores.

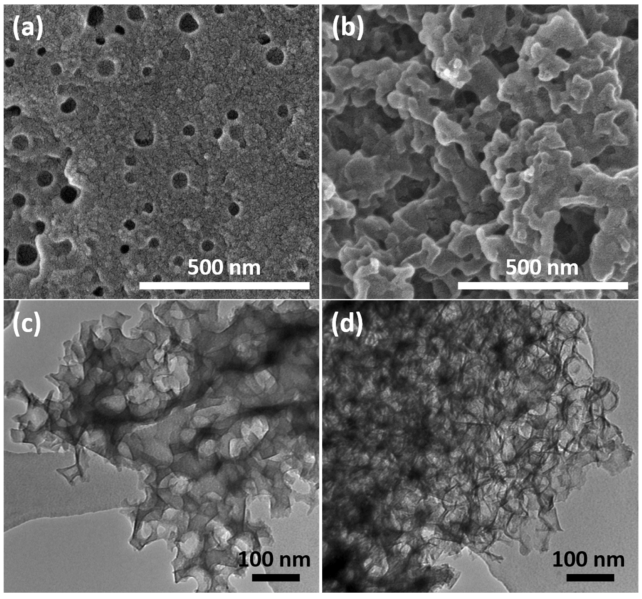

Figure 1. SEM images of (a) HPC-1 and (b) HPC-4; TEM images of (c) HPC-1 and (d) HPC-4.

Figure 2 shows the N_2 adsorption−desorption isotherms of HPCs with different ZnO/pitch weight ratios. It can be found that the isotherms of HPC are close to type IV according to the IUPAC classification, indicating the co-existence of micropores and mesopores formed in HPC. In addition, the hysteresis loop at a low relative pressure (0.4−0.8) could also prove the presence of mesopores. It is worth noting that the nitrogen adsorbed volume at a relative pressure (P/P_0) of 0.9 to 1.0 is significantly enhanced with the increase in the ZnO/pitch ratio. This result indicates that the pore structure of the carbon materials involves more and more meso- and macropores as the ZnO/pitch ratio increases. These results also could be confirmed by the pore size distribution curves of HPCs, shown in Figure 3. It clearly reveals the hierarchical pore structure of HPCs, composed of micropores, mesopores, and macropores. Furthermore, Figure 3b shows that the pore volume of HPCs at around 40 nm rises with the increase of ZnO mass, which advocates the important role of ZnO in the creation of mesopores and macropores.

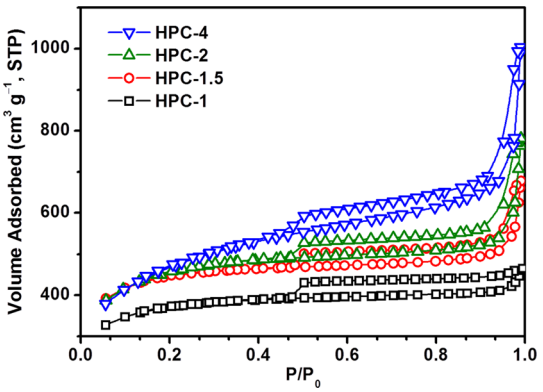

Figure 2. Nitrogen adsorption−desorption isotherms of HPCs. HPC-X (X = 1, 1.5, 2, and 4) indicates different ZnO/pitch ratios.

The Table 1 shows the textural parameters, yield, and tap density of the HPCs at different ZnO/pitch ratios. It can be found that the S_{BET} of HPC-1, HPC-1.5, HPC-2, and HPC-4 reaches 1141, 1347, 1469, and 1537 $m^2\ g^{-1}$, respectively, with the highest yield of 49%. The S_{BET} of HPCs slight increases when the ZnO mass increases. Furthermore, it is also observed that the pore size and pore volume enlarge from 2.4 to 3.7 nm and 0.691 to 1.41 g cm^{-3}, respectively, with the increase in the ZnO/pitch ratio. It is because ZnO is a spherical particle with a diameter of 20−30 nm that can create holes of several tens of nanometers as mesopores and macropores in carbon structures through casting. Again, this result importantly demonstrates that pore size and pore volume of the carbon materials could be well-controlled by adjusting the ratio of ZnO/pitch. In other words, HPCs with a larger pore size and pore volume, which is favorable to ion transportation, can be easily obtained by only increasing the ZnO/pitch ratio.

Notwithstanding that most characteristics of HPCs can be significantly improved by raising the amount of ZnO, it was

https://doi.org/10.1021/acsomega.2c04119
ACS Omega 2022, 7, 47610−47618

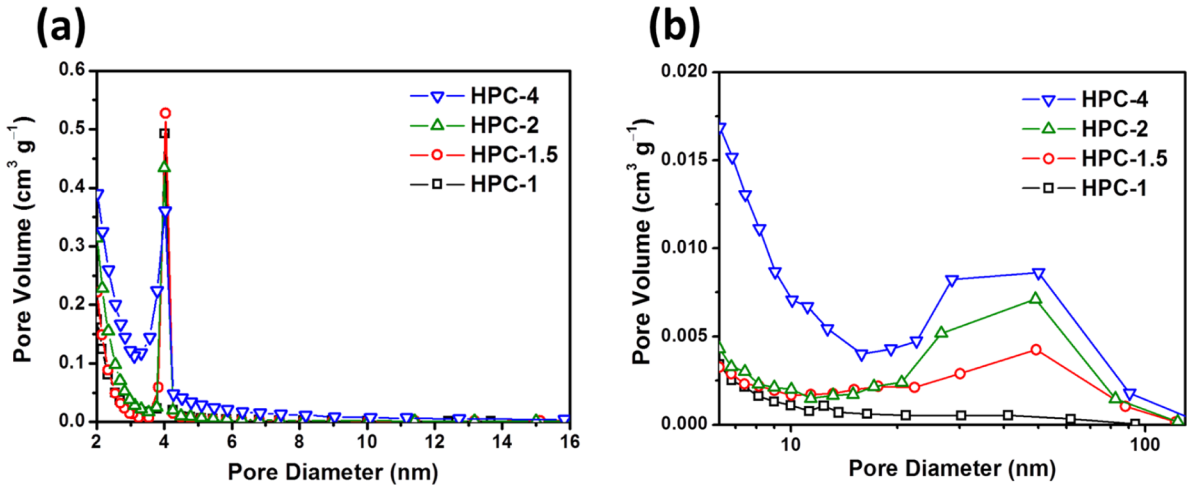

Figure 3. (a) 2−16 nm and (b) 6−130 nm pore size distribution curves of HPC after different treatments. HPC-*X* (*X* = 1, 1.5, 2, and 4) indicates different ZnO/pitch ratios.

Table 1. Influence of the ZnO/Pitch Ratio on Textural Properties of HPCs

sample	S_{BET}[a] (m^2g^{-1})	S_{ext}[b] (m^2g^{-1})	D_{ap}[c] (nm)	V_t[d] (cm^3g^{-1})	V_{ext}[e] (cm^3g^{-1})	% of V_{ext}[f]	D_{tap}[g] ($g^{-1}cm^{-3}$)	yield[h] (%)
HPC-1	1141	357	2.4	0.69	0.27	39	0.57	49
HPC-1.5	1347	384	2.9	0.97	0.45	46	0.42	49
HPC-2	1469	607	3.1	1.10	0.66	60	0.31	46
HPC-4	1537	994	3.7	1.41	1.12	79	0.20	40

[a]BET specific surface area determined by the BET method. [b]External surface area >2 nm. [c]Average pore diameter ($D_{ap} = 4V_t/S_{BET}$). [d]Total pore volume measured at $P/P_0 = 0.99$. [e]External pore volume >2 nm. [f]$(V_{ext}/V_t) \times 100$. [g]Tap density. [h]Weight of carbon/weight of pitch.

found from Figure 4 that the tap density of HPCs would dramatically decrease from 0.57 to 0.20 g cm^{-3}. That is,

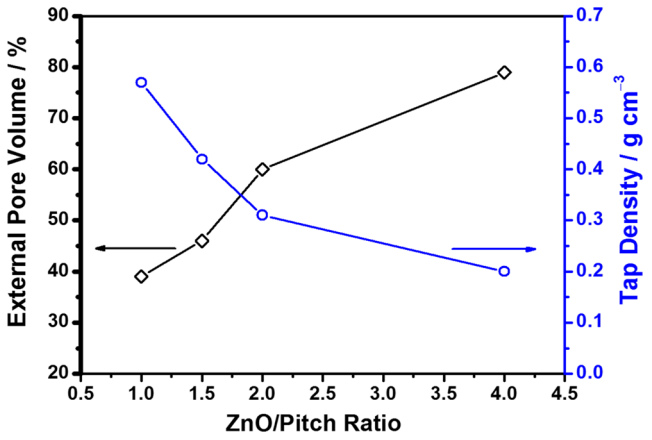

Figure 4. External pore volume and tap density, respectively, of different ZnO/pitch ratios.

although the S_{BET}, pore size, and pore volume of HPC-4 can reach 1537 cm^3 g^{-1}, 3.7 nm, and 1.41 g cm^{-3}, respectively, by increasing the ratio of ZnO/pitch, the tap density of HPC-4 would fall to 0.20 g cm^{-3}. The tap density is an important factor that would decide whether the materials can be heavily coated onto current collectors. As in this research, the tap density of HPC-4 is too low to be used as an electrode material for CDI devices. Under the same carbon loading, the HPC-4 electrode would seriously crack or even separate from the current collector (Figure 5).

3.2. Electrochemical Properties. Figure 6a−c shows the CV curves of HPC-1, HPC-1.5, and HPC-2 electrodes,

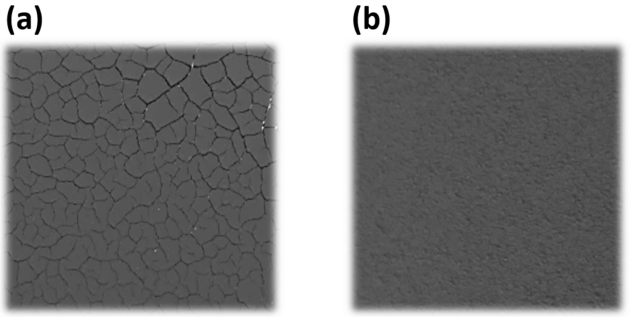

Figure 5. Pictures of (a) HPC-4 and (b)HPC-2 coating on the current collector.

respectively, at different scan rates including 5, 10, 20, 50, 100, 200, and 500 mV s^{-1} with a potential range of 0 to 1.0 V in 1.0 M $NaCl_{(aq)}$ solution. All CV curves are close to rectangular without any oxidation/reduction peaks appearing, suggesting the absence of a Faradaic reaction and the reversibility of the electrosorption process. Figure 6d reveals the CV curves of these electrodes at a potential sweep rate of 500 mV s^{-1} for comparison. It can be found that the HPC-2 is nearest to a rectangle shape and involves the largest integrated area among these electrodes, which means that HPC-2 has the best capacitive behavior and the greatest ion storage capacity at the scan rate of 500 mV s^{-1}.

This result can also be confirmed by the galvanostatic charge/discharge (GC) test shown in Figure 7a. All GC curves are symmetric triangular shapes, manifesting that their behavior is ideal ions electro-absorption−desorption rather than Faradic reaction. Moreover, the discharging time of HPC-2 is the longest among that of the other electrodes, which indicates the highest specific capacitance at 9 A g^{-1}. As shown

https://doi.org/10.1021/acsomega.2c04119
ACS Omega 2022, 7, 47610−47618

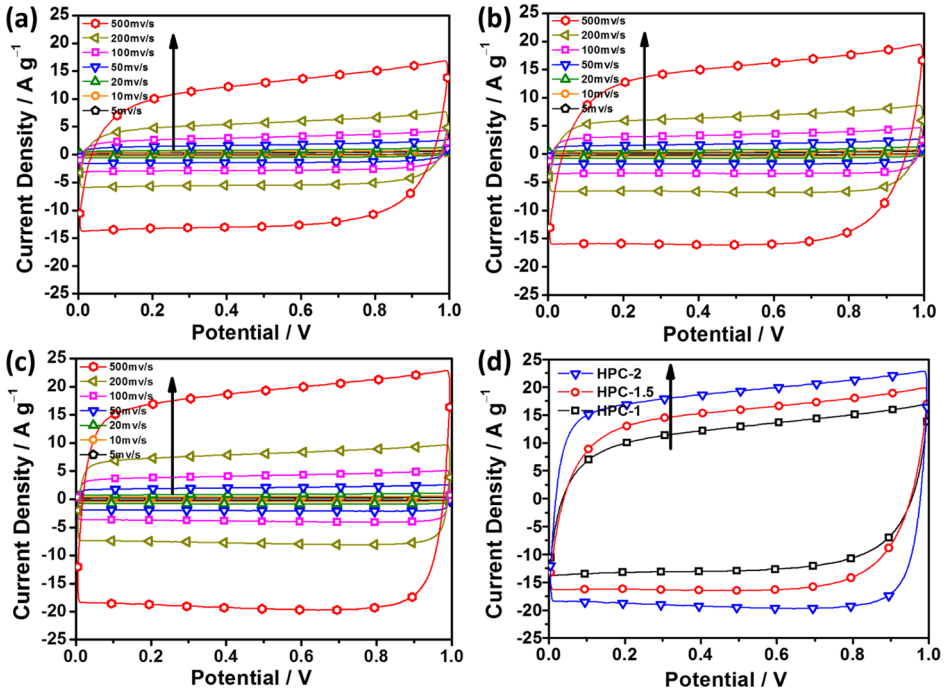

Figure 6. CV curves of (a) HPC-1, (b) HPC-1.5, and (c) HPC-2 at different potential scan rates; (d) typical CV curves at 500 mV s^{-1} in the 1.0 M $NaCl_{(aq)}$.

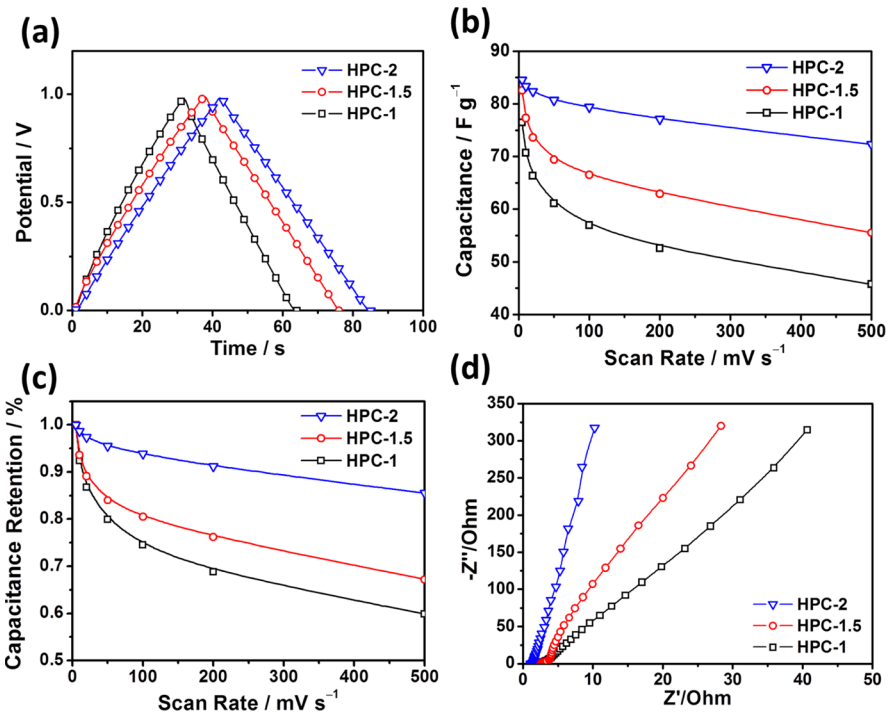

Figure 7. (a) GC curves with a current density of 9 A g^{-1}, (b) specific capacitance, (c) capacitance retention vs the voltage scan rate, and (d) Nyquist impedance plots for the HPC-1, HPC-1.5, and HPC-2 electrodes in 1.0 M $NaCl_{(aq)}$.

in Figure 7b,c, the specific capacitances of HPC-1, HPC-1.5, and HPC-2 at 5 mV s^{-1} are 77, 83, and 85 F g^{-1}, respectively. This slight increase in specific capacitance is due to the enhancement of the specific surface area. In addition, the HPC-2 electrode with V_{ext} of 60% exhibits the highest capacitance retention of 86% at 500 mV s^{-1}, indicating that the higher percentage of V_{ext} could significantly raise the capacitance retention of HPC at high scan rates. In other words, the formation of mesopores and macropores via the ZnO template could effectively relieve the EDL overlapping effect, shorten the ion diffusion distance, and lower the ion transport resistance. This result can also be proved by the EIS measurements. The Nyquist plots of the HPC-1, HPC-1.5, and HPC-2 were measured at 0 V and fitted to the Randles equivalent circuits involving resistance of solution (R_s), double-layer capacitance at the surface of the electrode (C_{dl}),

https://doi.org/10.1021/acsomega.2c04119
ACS Omega 2022, 7, 47610−47618

charge transfer resistance (R_{ct}), and Warburg resistance (Z_w) (Figure 7d). It can be found from the semicircle in the high-frequency region that the R_{ct} of HPC-1, HPC-1.5, and HPC-2 are 0.4, 0.8, and almost 0.0 Ω, respectively, indicating that HPC-2 has the lowest ion resistance, which shows the mobility of ionic electrolyte inside the textual pores of the electrode and the electronic resistance of electrode material. In addition, the obviously larger slope of HPC-2 in the low-frequency region suggests an ideal diffusion process at the electrode−electrolyte interface. Therefore, the hierarchical porous carbon with the optimum ratio of micropores to mesopores is beneficial for rapid ion electro-absorption−desorption behavior to achieve high ion storage capacity in a short time.

3.3. CDI Performance. The desalination performance of the prepared electrodes was investigated in batch-mode CDI experiments. The results indicated that the adsorption capacities of HPC-1, HPC-1.5, and HPC-2 were 8.17, 8.81, and 10.62 mg g^{-1}, respectively. As shown in Table 1, the specific surface area of HPC electrodes increased from 1141 m^2 g^{-1} (HPC-1) to 1469 m^2 g^{-1} (HPC-2) with the increasing amount of ZnO. It is believed that a high available surface area of the used carbonaceous material can lead to a high adsorption capacity of the prepared electrode.[37] Therefore, the increment in adsorption capacity can be attributed to the increased specific surface area of HPC.

Importantly, HPC-2 presented a significant improvement in adsorption capacity in the early stage of the electrosorption process (as shown in Figure 8). A high adsorption capacity of

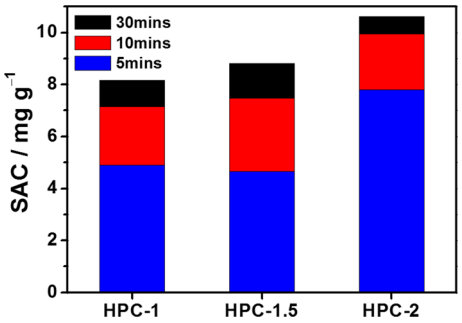

Figure 8. Salt adsorption capacities of HPC-*X* in a 5.0 mM NaCl solution.

9.94 mg g^{-1} means 93.6% of the maximum adsorption capacity (10.62 mg g^{-1}) of HPC-2 can be reached in the first 10 min. The maximum average SAR (Figure 9) in the duration of the electrosorption process for HPC-2 was 1.77 mg g^{-1} min^{-1},

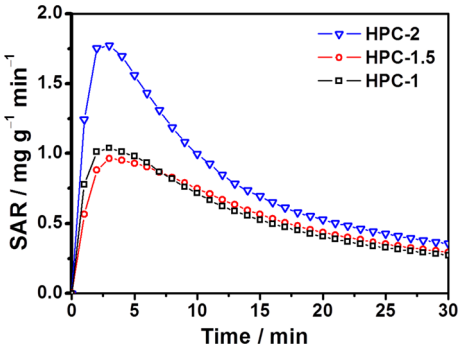

Figure 9. SARs of HPC-*X* in a 5.0 mM NaCl solution.

which was higher than that of other investigated electrodes. As demonstrated by Li et al.,[38] electrodes present a better rate capability when the mesopore fractions are higher than 50%. In this study, the mesopore fraction of HPC-2 is as high as 60%. The charged ions can diffuse easily into the mesopores of the electrode; then, the double layer at the carbon-electrolyte interface is primarily formed in the mesopore region.[39] Furthermore, mesopores can act as entries to micropores and are useful for ion transportation.[40] Therefore, good pore accessibility of the electrodes also benefits the electrosorption behavior in the micropore region. Figure 10 clearly indicates

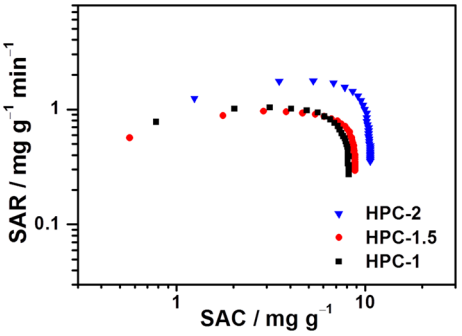

Figure 10. CDI Ragone plots for HPC-*X* in a 5.0 mM NaCl solution.

that both the adsorption rate and adsorption capacity of HPC-2 were higher than those of HPC-1 and HPC-1.5. It can be concluded that the improvement in the desalination performance of HPC-2 resulted from its enhanced accessibility of pores with the electrolyte ions. Noteworthily, even in a low concentration NaCl solution of 1.0 mM, HPC-2 still possesses a high SAC, namely 7.85 mg g^{-1}, which is a superior performance compared with that of other common electrodes reported in the literature (Table 2), including OMC (0.54 mg g^{-1}), AC (0.28 mg g^{-1}), hierarchical ACF (4.8 mg g^{-1}), CNT (0.87 mg g^{-1}), and graphene (1.34 mg g^{-1}). This result advocates the outstanding desalination performance of HPC-2 over other porous carbon materials.

A consecutive electrosorption/regeneration experiment was conducted in a 5 mM NaCl aqueous solution at 1.2/0.0 V to evaluate the electrochemical stability and regeneration performance of HPC-2. As shown in Figure 11, the desalination performance remains stable after three consecutive cycles of electrosorption/regeneration. The result indicated that electrodes made from HPC-2 present high electrochemical stability. The conductivity decreased greatly at the beginning of the electrosorption. The charged ions in the solution were electrostatically adsorbed and transported to the electrode surface under the influence of an electric field in the electrosorption process. Then, the charged ions were stored in EDLs at the carbon-electrolyte interface. Consequently, the conductivity was stabilized because the electrode was saturated with ions. In the desorption process, the external electric field was removed, and the ions were diffused from the carbon-electrolyte interface to the bulk solution based on a concentration gradient. The desorption efficiencies for each cycle were 100, 95.8, and 95.7%. The high desorption efficiency evidenced that the removal mechanism in the electrosorption process was mainly conducted by electrosorption.

https://doi.org/10.1021/acsomega.2c04119
ACS Omega 2022, 7, 47610−47618

Table 2. Comparison of Salt Adsorption Capacities of Porous Carbon Electrodes for Low Concentration NaCl Solution

carbon electrode	S_{BET}(m^2g^{-1})	V_t(cm^3g^{-1})	working voltage (V)	initial $NaCl_{(aq)}$ concentration (mM)	SAC (mg g^{-1})	references
OMC	1594	1.45	0.8	~0.8	0.54	41
AC	845	0.61	0.8	~0.8	0.28	41
hierarchical ACF	656	0.39	1.6	~1.54	4.80	42
hierarchical OMC	410		1.2	~68	13.95	43
3DGHPC	384	0.73	1.2	~0.43	6.18	44
3DG	250	0.49	1.2	~0.43	4.41	44
graphene	222	51.01	2	~0.43	1.34	45
DWCNT	415		2	~0.4	0.75	46
SWCNT	453		2	~0.4	0.55	46
CNT	449	0.19	0.8	~0.8	0.19	47
			1.2	~0.8	0.58	
			1.6	~0.8	0.87	
HPC-2	1469	1.10	1.2	1	7.85	this work
				5	10.62	

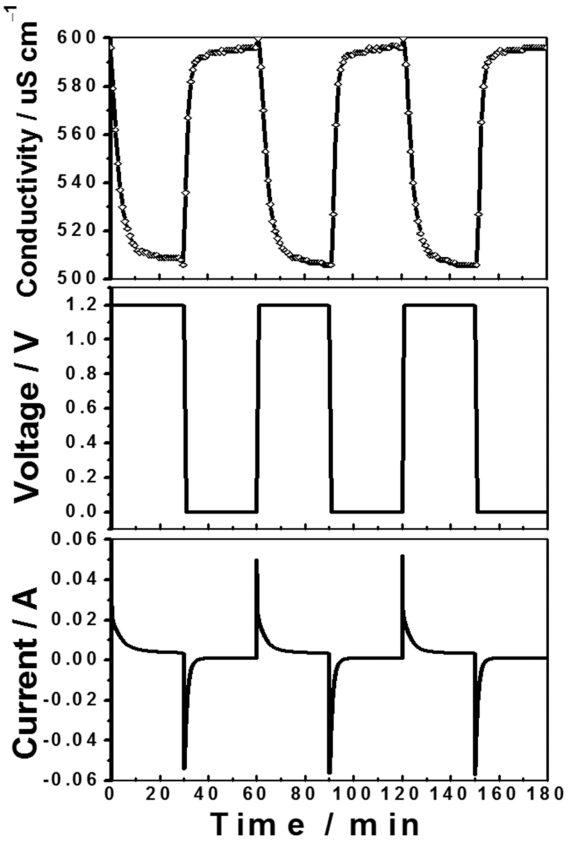

Figure 11. Multiple electrosorption/regeneration cycles in a 5.0 mM NaCl solution for the (a) working voltage, (b) current, and (c) conductivity measurements.

4. CONCLUSIONS

In this study, HPCs with a high specific surface area and well-connected pore channels were synthesized through a solvent-free ZnO-template method. Importantly, the micro/mesopore ratio and density of HPCs can be easily tailored by only adjusting the ZnO/pitch ratio. Due to the traits of simplicity, low cost, environmentally friendly, and feasible control of pore structure, this process has possessed a huge potential for further commercialization. In the electrochemical analysis, the HPC-2 exhibits a supreme capacitive behavior with high specific capacitance and capacitance retention. The high proportion of mesoporous channels in HPC-2 allows a significantly low inner resistance to ion transportation. For water desalination, the HPC-2 has a high salt absorption capacity of 10.62 mg g^{-1} in 5 mM $NaCl_{(aq)}$ at an applied voltage of 1.2 V. Noteworthily, the salt absorption capacity of HPC-2 could reach 9.94 mg g^{-1} within the first 10 min, with a high maximum salt absorption rate of 1.77 mg g^{-1} min^{-1}, which is beneficial to shorten the time of a cycle on water desalination. Moreover, the HPC-2 electrode exhibits superior performance to electroadsorb salt ions from low concentration of the solution (1 mM $NaCl_{(aq)}$), with an electrosorption capacity of 7.85 mg g^{-1} at an applied voltage of 1.2 V. These results show the potential of the HPC-2 electrode for rapid water desalination and emphasize the importance of micro/mesopore ratio control for achieving optimized SAC. Furthermore, HPC-*X* electrodes can also be a promising material for large-scale capacitive charge storage devices and electroactive sorbents with favorable ion transportation.

AUTHOR INFORMATION

Corresponding Authors

Chia-Hung Hou − *Graduate Institute of Environmental Engineering, National Taiwan University, Taipei 106, Taiwan*; orcid.org/0000-0001-5149-4096; Email: chiahunghou@ntu.edu.tw

Hong-Ping Lin − *Department of Chemistry, National Cheng Kung University, Tainan 701, Taiwan*; orcid.org/0000-0001-9021-3146; Email: hplin@mail.ncku.edu.tw

Authors

Guan-Wen Liu − *Department of Chemistry, National Cheng Kung University, Tainan 701, Taiwan*

Chen-Shiuan Fan − *Graduate Institute of Environmental Engineering, National Taiwan University, Taipei 106, Taiwan*

Chun-Han Hsu − *General Education Center, Nation Tainan Junior College of Nursing, Tainan 700, Taiwan*

Complete contact information is available at: https://pubs.acs.org/10.1021/acsomega.2c04119

Notes

The authors declare no competing financial interest.

ACKNOWLEDGMENTS

This work was supported by the Ministry of Science and Technology, Taiwan, for the generous financial support of this

https://doi.org/10.1021/acsomega.2c04119
ACS Omega 2022, 7, 47610−47618

research under contract nos. (MOST 110-2113-M-006-017 and MOST 110-2622-E-006-001-CC1).

REFERENCES

(1) Suss, M. E.; Porada, S.; Sun, X.; Biesheuvel, P. M.; Yoon, J.; Presser, V. Water Desalination via Capacitive Deionization: What Is It and What Can We Expect From It? *Energy Environ. Sci.* **2015**, *8*, 2296−2319.
(2) Anderson, M. A.; Cudero, A. L.; Palma, J. Capacitive Deionization as an Electrochemical Means of Saving Energy and Delivering Clean Water. Comparison to Present Desalination Practices: Will it Compete? *Electrochim. Acta* **2010**, *55*, 3845−3856.
(3) Porada, S.; Zhao, R.; van der Wal, A.; Presser, V.; Biesheuvel, P. M. Review on the Science and Technology of Water Desalination by Capacitive Deionization. *Prog. Mater. Sci.* **2013**, *58*, 1388−1442.
(4) Salari, K.; Zarafshan, P.; Khashehchi, M.; Chegini, G.; Etezadi, H.; Karami, H.; Szulżyk-Cieplak, J.; Łagód, G. Knowledge and Technology used in Capacitive Deionization of Water. *Membranes* **2022**, *12*, 459.
(5) Xu, P.; Drewes, J. E.; Heil, D.; Wang, G. Treatment of Brackish Produced Water Using Carbon Aerogel-Based Capacitive Deionization Technology. *Water Res.* **2008**, *42*, 2605−2617.
(6) Wen, X. R.; Zhang, D. S.; Shi, L. Y.; Yan, T. T.; Wang, H.; Zhang, J. P. Three-Dimensional Hierarchical Porous Carbon with a Bimodal Pore Arrangement for Capacitive Deionization. *J. Mater. Chem.* **2012**, *22*, 23835−23844.
(7) Wang, X. Q.; Lee, J. S.; Tsouris, C.; DePaoli, D. W.; Dai, S. Preparation of Activated Mesoporous Carbons for Electrosorption of Ions from Aqueous Solutions. *J. Mater. Chem.* **2010**, *20*, 4602−4608.
(8) Tsai, S. W.; Hackl, L.; Kumar, A.; Hou, C. H. Exploring the Electrosorption Selectivity of Nitrate over Chloride in Capacitive Deionization (CDI) amd membrane capacitive deionization (MCDI). *Desalination* **2021**, *497*, 114764.
(9) Humplik, T.; Lee, J.; O'Hern, S. C.; Fellman, B. A.; Baig, M. A.; Hassan, S. F.; Atieh, M. A.; Rahman, F.; Laoui, T.; Karnik, R.; Wang, E. N. Nanostructured Materials for Water Desalination. *Nanotechnology* **2011**, *22*, 292001.
(10) Zhang, D. S.; Shi, L. Y.; Fang, J. H.; Dai, K.; Liu, J. Q. Influence of Carbonization of Hot-Pressed Carbon Nanotube Electrodes on Removal of NaCl from Saltwater Solution. *Mater. Chem. Phys.* **2006**, *96*, 140−144.
(11) Wang, L.; Wang, M.; Huang, Z. H.; Cui, T. X.; Gui, X. C.; Kang, F. Y.; Wang, K. L.; Wu, D. H. Capacitive Deionization of NaCl Solutions Using Carbon Nanotube Sponge Electrodes. *J. Mater. Chem.* **2011**, *21*, 18295−18299.
(12) Villar, I.; Roldan, S.; Ruiz, V.; Granda, M.; Blanco, C.; Menéndez, R.; Santamaría, R. Capacitive Deionization of NaCl Solutions with Modified Activated Carbon Electrodes. *Energy Fuels* **2010**, *24*, 3329−3333.
(13) Li, Y.; Hussain, I.; Qi, J. W.; Liu, C.; Li, J. S.; Shen, J. Y.; Sun, X. Y.; Han, W. Q.; Wang, L. J. N-doped Hierarchical Porous Carbon Derived from Hypercrosslinked Diblock Copolymer for Capacitive Deionization. *Sep. Purif. Technol.* **2016**, *165*, 190−198.
(14) Baroud, T. N.; Giannelis, E. P. High Salt Capacity and High Removal Rate Capacitive Deionization Enabled by Hierarchical Porous Carbons. *Carbon* **2018**, *139*, 614−625.
(15) Wen, X. R.; Zhang, D. S.; Yan, T. T.; Zhang, J. P.; Shi, L. Y. Three-Dimensional Graphene -Based Hierarchically Porous Carbon Composites Prepared by a Dual-Template Strategy for Capacitive Deionization. *J. Mater. Chem. A* **2013**, *1*, 12334−12344.
(16) Xu, J. Q.; Zhou, K.; Chen, F.; Chen, W.; Wei, X. F.; Liu, X. W.; Liu, J. H. Natural Integrated Carbon Architecture for Rechargeable Lithium-Sulfur Batteries. *ACS Sustainable Chem. Eng.* **2016**, *4*, 666−670.
(17) Tang, C.; Li, B. Q.; Zhang, Q.; Zhu, L.; Wang, H. F.; Shi, J. L.; Wei, F. CaO-Templated Growth of Hierarchical Porous Graphene for High-Power Lithium−Sulfur Battery Applications. *Adv. Funct. Mater.* **2016**, *26*, 577−585.
(18) Zhang, X. Y.; Wang, X. Y.; Su, J. C.; Wang, X. Y.; Jiang, L. L.; Wu, H.; Wu, C. The Effects of Surfactant Template Concentration on the Supercapacitive Behaviors of Hierarchically Porous Carbons. *J. Power Sources* **2012**, *199*, 402−408.
(19) Studart, A. R.; Studer, J.; Xu, L.; Yoon, K.; Shum, H. C.; Weitz, D. A. Hierarchical Porous Materials Made by Drying Complex Suspensions. *Langmuir* **2011**, *27*, 955−964.
(20) Zhao, B.; Collinson, M. M. Well-Defined Hierarchical Templates for Multimodal Porous Material Fabrication. *Chem. Mater.* **2010**, *22*, 4312−4319.
(21) Liang, C. D.; Li, Z. J.; Dai, S. Mesoporous Carbon Materials: Synthesis and Modification. *Angew. Chem., Int. Ed.* **2008**, *47*, 3696−3717.
(22) Hsu, C. H.; Pan, Z. B.; Chen, C. R.; Wei, M. X.; Chen, C. A.; Lin, H. P.; Hsu, C. H. Synthesis of Multiporous Carbons from the Water Caltrop Shell for High-Performance Supercapacitors. *ACS Omega* **2020**, *5*, 10626−10632.
(23) Wu, S. H.; Mou, C. Y.; Lin, H. P. Synthesis of Mesoporous Silica Nanoparticles. *Chem. Soc. Rev.* **2013**, *42*, 3862−3875.
(24) Liu, G. W.; Chen, T. Y.; Chung, C. H.; Lin, H. P.; Hsu, C. H. Hierarchical Micro/Mesoporous Carbons Synthesized with a ZnO Template and Petroleum Pitch via a Solvent-Free Process for a High-Performance Supercapacitor. *ACS Omega* **2017**, *2*, 2106−2113.
(25) Frank, E.; Steudle, L. M.; Ingildeev, D.; Spörl, J. M.; Buchmeiser, M. R. Carbon Fibers: Precursor Systems, Processing, Structure, and Properties. *Angew. Chem., Int. Ed.* **2014**, *53*, 5262−5298.
(26) Liu, Y. D.; Kumar, S. Polymer Reviews Recent Progress in Fabrication, Structure, and Properties of Carbon Fibers. *Polym. Rev.* **2012**, *52*, 234−258.
(27) Inagaki, M.; Qiu, J. S.; Guo, Q. G. Carbon Foam: Preparation and Application. *Carbon* **2015**, *87*, 128−152.
(28) Inagaki, M.; Toyoda, M.; Soneda, Y.; Tsujimura, S.; Morishita, T. Templated Mesoporous Carbons: Synthesis and Applications. *Carbon* **2016**, *107*, 448−473.
(29) Wang, Y. X.; Chou, S. L.; Kim, J. H.; Liu, H. K.; Dou, S. X. Nanocomposites of Silicon and Carbon Derived From Coal Tar Pitch: Cheap Anode Materials for Lithium-Ion Batteries with Long Cycle Life and Enhanced Capacity. *Electrochim. Acta* **2013**, *93*, 213−221.
(30) Li, Z.; Wu, Y. J.; Zhao, Y.; Wang, L. X.; Zhu, H. S.; Qin, L. J.; Feng, F. F.; Wang, W.; Wu, Y. M. Analysis of Coal Tar Pitch and Smoke Extract Components and Their Cytotoxicity on Human Bronchial Epithelial Cells. *J. Hazard. Mater.* **2011**, *186*, 1277−1282.
(31) Lao, R. C.; Thomas, R. S.; Monkman, J. L. Computerized Gas Chromatographic-Mass Spectrometric Analysis of Polycyclic Aromatic Hydrocarbons in Environmental Samples. *J. Chromatogr. A* **1975**, *112*, 681−700.
(32) Phuoc, N. M.; Jung, E. Y.; Tran, N. A. T.; Lee, Y. W.; Yoo, C. Y.; Kang, B. G.; Cho, Y. Ehanced Desalination Performance of Capacitive Deionization using Nanoporous Carbon Derived from ZIF-67 Metal Organic Frameworks and CNTs. *Nanomaterials* **2020**, *10*, 2091.
(33) Baek, J.; An, K. H.; Chung, D. C.; Kim, B.-J. Correlation Studies between Pore Structure and Electrochemical Performance of Activated Polymer-Based Hard Carbon with Various Organic and Aqueous Electrolytes. *Int. J. Energy Res.* **2018**, *42*, 2927−2939.
(34) Zhang, J. S.; Lee, J. W. Supercapacitor Electrodes Derived from Carbon Dioxide. *ACS Sustainable Chem. Eng.* **2014**, *2*, 735−740.
(35) Lee, J.-H.; Bae, W.-S.; Choi, J.-H. Electrode Reactions and Adsorption/Desorption Performance Related to The Applied Potential in A Capacitive Deionization Process. *Desalination* **2010**, *258*, 159−163.
(36) Chuenchom, L.; Kraehnert, R.; Smarsly, B. M. Recent Progress in Soft-Templating of Porous Carbon Materials. *Soft Matter* **2012**, *8*, 10801−10812.
(37) Ying, T.-Y.; Yang, K.-L.; Yiacoumi, S.; Tsouris, C. Electrosorption of Ions from Aqueous Solutions by Nanostructured Carbon Aerogel. *J. Colloid Interface Sci.* **2002**, *250*, 18−27.

https://doi.org/10.1021/acsomega.2c04119
ACS Omega 2022, 7, 47610−47618

(38) Li, L.; Song, H.; Chen, X. Pore Characteristics and Electrochemical Performance of Ordered Mesoporous Carbons for Electric Double-Layer Capacitors. *Electrochim. Acta* **2006**, *51*, 5715−5720.
(39) Gabelich, C. J.; Tran, T. D.; Suffet, I. H. Electrosorption of Inorganic Salts from Aqueous Solution Using Carbon Aerogels. *Environ. Sci. Technol.* **2002**, *36*, 3010−3019.
(40) Gryglewicz, G.; Machnikowski, J.; Lorenc-Grabowska, E.; Lota, G.; Frackowiak, E. Effect of Pore Size Distribution of Coal-Based Activated Carbons on Double Layer Capacitance. *Electrochim. Acta* **2005**, *50*, 1197−1206.
(41) Li, L.; Zou, L.; Song, H.; Morris, G. Ordered Mesoporous Carbons Synthesized by a Modified Sol−Gel Process for Electrosorptive Removal of Sodium Chloride. *Carbon* **2009**, *47*, 775−781.
(42) Wang, G.; Dong, Q.; Ling, Z.; Pan, C.; Yu, C.; Qiu, J. Hierarchical Activated Carbon Nanofiber Webs with Tuned Structure Fabricated by Electrospinning for Capacitive Deionization. *J. Mater. Chem.* **2012**, *22*, 21819−21823.
(43) Mayes, R. T.; Tsouris, C.; Kiggans, J. O.; Mahurin, S. M.; Depaoli, D. W.; Dai, S. Hierarchical Ordered Mesoporous Carbon from Phloroglucinol - Glyoxal and Its Application in Capacitive Deionization of Brackish Water. *J. Mater. Chem.* **2010**, *20*, 8674−8678.
(44) Wen, X.; Zhang, D.; Yan, T.; Zhang, J.; Shi, L. Three-Dimensional Graphene-Based Hierarchically Porous Carbon Composites Prepared by a Dual-Template Strategy for Capacitive Deionization. *J. Mater. Chem. A* **2013**, *1*, 12334−12344.
(45) Li, H.; Zou, L.; Pan, L.; Sun, Z. Novel Graphene-like Electrodes for Capacitive Deionization. *Environ. Sci. Technol.* **2010**, *44*, 8692−8697.
(46) Li, H.; Pan, L.; Lu, T.; Zhan, Y.; Nie, C.; Sun, Z. A Comparative Study on Electrosorptive Behavior of Carbon Nanotubes and Graphene for Capacitive Deionization. *J. Electroanal. Chem.* **2011**, *653*, 40−44.
(47) Li, H.; Liang, S.; Li, J.; He, L. The Capacitive Deionization Behaviour of a Carbon Nanotube and Reduced Graphene Oxide Composite. *J. Mater. Chem. A* **2013**, *1*, 6335−6341.

https://doi.org/10.1021/acsomega.2c04119
ACS Omega 2022, 7, 47610−47618